




# Floquet engineering tunable periodic gauge fields and simulating real topological phases in a cold-alkaline-earth-metal-atom optical lattice

Wei Wang <sup>1,2</sup> Zheng Zhang,<sup>3</sup> Gui-Xin Tang <sup>4</sup> and Tao Wang <sup>1,2,5,\*</sup>

<sup>1</sup>*Department of Physics and Chongqing Key Laboratory for Strongly Coupled Physics, Chongqing University, Chongqing 401331, China*

<sup>2</sup>*Center of Modern Physics, Institute for Smart City of Chongqing University in Liyang, Liyang 213300, China*

<sup>3</sup>*National Laboratory of Solid State Microstructures and Department of Physics, Nanjing University, Nanjing 210093, China*

<sup>4</sup>*Center of Ultra-precision Optoelectronic Instrument Engineering, Harbin Institute of Technology, Harbin 150001, China*

<sup>5</sup>*State Key Laboratory of Quantum Optics and Quantum Optics Devices, Shanxi University, Taiyuan 030006, China*



(Received 19 April 2024; accepted 12 July 2024; published 6 August 2024)

We propose to synthesize tunable periodic gauge fields via Floquet engineering cold-alkaline-earth-metal atoms in one-dimensional optical lattice. The artificial magnetic flux is designed to emerge during the combined process of Floquet photon-assisted tunneling and internal state transitions. By varying the initial phases of the driving protocol, our proposal presents the ability to smoothly tune the periodic flux. Moreover, we demonstrate that the effective two-leg flux ladder model can simulate one typical real topological insulator, which is described by the first Stiefel-Whitney class and protected by the space-inversion-time-reversal symmetry. Benefiting from the long lifetime of excited states of alkaline-earth-metal atoms, our work opens new possibilities for exploiting the physics related to gauge fields, such as topological phases, in the current cold-atom platform.

DOI: [10.1103/PhysRevA.110.023308](https://doi.org/10.1103/PhysRevA.110.023308)

## I. INTRODUCTION

Gauge fields, as well as the associated gauge theories, are crucial to modern physics. In the standard model, complex gauge fields are necessary to mediate the interactions between elementary particles. The application of strong magnetic fields to two-dimensional electronic systems has led to the discovery of topological matter [1–5] that has been actively expanded over the past 15 years [6–10]. Among the topological matter, Chern insulators have drawn tremendous attention for exploring the topological mechanisms beyond Landau levels and their potential application aspects, which was first proposed by Haldane through introducing staggered fluxes threading the honeycomb lattice [11]. Inspired by this spatial magnetic configuration, much research has been devoted to combining that with various lattice systems, whose interplay results in flat bands [12–18], anomalous quantum Hall effects [12,19,20], high Chern numbers [15,18], high-order Chern number [17], unique edge states [21,22], and so on. Extra effort has focused on investigating other periodic fluxes to explore similar phenomena such as high Chern numbers [23], redistribution of Chern numbers [24,25], and chiral edge states [26]. Nevertheless, it is interesting to note that there is a kind of novel topological phase recently emerging from the periodic  $\pi$  flux configuration [27–35]. Distinct from other precursors, their Brillouin zone, band topologies, edge states, symmetry groups, and topological classifications are profoundly modified by the  $Z_2$  projective algebra [27–32]. It is naturally anticipated that more general periodic  $U(1)$  gauge fields may extend the realm of intriguing topological

phases [28]. However, how to engineer periodic gauge fields is still an open question.

Due to the unprecedentedly clean and controllable experimental system, cold atoms offer a unique platform for simulating and investigating the gauge fields [36–41]. One early and simple route to synthesizing effective magnetic fields involves rapidly rotating the cold gases, leveraging the analogy between the neutral atomic Coriolis force and the charged particles' Lorentz force [42–46]. This method, however, faces a limitation in the range of the fields it can induce. To approach larger gauge fields, the scheme of laser-assisted tunneling was later suggested to exploit Peierls phases which arise when the suppressed adjacent tunneling is resonantly restored by Raman transitions [47–52]. Widely used with alkali-metal atoms, such scenarios typically generate staggered or uniform gauge fields. Desirable are the diverse spatial configurations. A more elaborate dynamical driving technique, commonly referred to as Floquet engineering [41,53–63], can be employed to achieve gauge fields of varied lattice configurations, attaching gauge fields to a triangular lattice, a kagome lattice, and a hexagonal lattice [56,57,61,64–66]. The proven versatile tool can even engineer solenoid-type flux geometries [67].

Among those cold atomic species, cold-alkaline-earth-metal atoms (AEMAs) offer unique advantages for simulating gauge fields. The primary reason is that, by utilizing long-lived electronic excited states, the strongly suppressed spontaneous emission reduces related heating [50,68–72]. This useful low heating rate has allowed the application of Floquet engineering methods in optical lattices to advance recent experimental progress not only in quantum simulation but also in precision measurement [73,74]. These developments motivate us to explore the possibility of engineering periodic artificial gauge fields in such atomic platforms.

\*Contact author: tauwaang@cqu.edu.cn

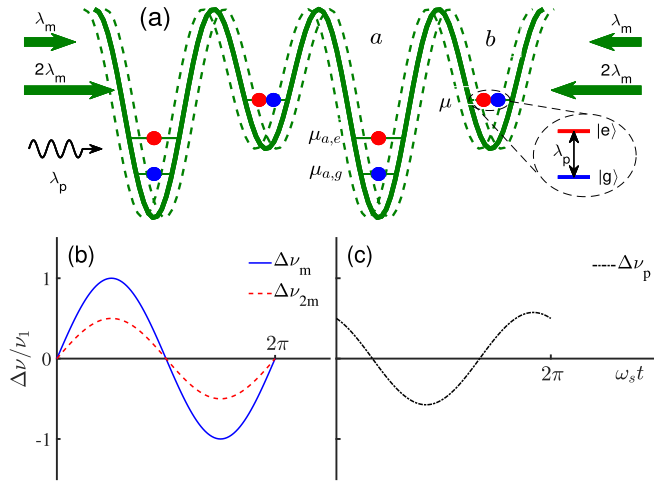


FIG. 1. Sketch of the proposed setup. (a) Cold AEMAs are trapped in a shaking superlattice formed by two standing-wave laser fields with wavelengths  $\lambda_m$  and  $2\lambda_m$ . Interacting with modulated pumping lasers, atoms with ground states  $|g\rangle$  can be excited to higher-energy levels  $|e\rangle$ . (b) Periodic shaking of superlattice originates from the two coordinated frequency modulation functions for the laser with magic wavelength  $\Delta\nu_m = v_1 \sin(\omega_s t)$  and the other  $\Delta\nu_{2m} = \frac{v_1}{2} \sin(\omega_s t)$ , denoted by the blue solid line and red dashed line, respectively. (c) Modulation function to the frequency of the pumping laser  $\Delta\nu_p(t) = v_2 \cos(\omega_s t + \varphi) + \frac{\lambda_m}{2\lambda_p} v_1 \sin(\omega_s t)$ , with setting  $v_2 = v_1$ ,  $\varphi = \frac{\pi}{3}$ , and  $\frac{\lambda_m}{\lambda_p} = \frac{7\pi}{6}$ .

In this paper we propose a feasible and efficient scheme for the generation of tunable periodic gauge fields by Floquet engineering of cold AEMAs. Starting with the synthetic dimension method, we further break the spatial translation symmetry and periodically drive the system. By designing an appropriate superlattice, we show that these atoms experience state-dependent potentials, and thus acquire net magnetic fluxes attaching the artificial “electronic” dimension due to different Floquet photon-assisted resonant precesses. Intriguingly, it is found that the effective two-leg periodic flux model can exhibit the real topological phase. This topological state is protected by  $PT$  symmetry, the combined symmetry of spatial inversion  $P$  and time reversal  $T$ , and characterized by the first Stiefel-Whitney class. Topological phase transition can occur when tuning the periodic flux.

The paper is organized as follows. Section II serves as an introduction to our proposal and the corresponding time-dependent Floquet model. In Sec. III we discuss the effective Hamiltonian in the case of the Floquet photon-assisted resonant tunneling between adjacent sublattices and the transition between two levels of atoms. According to that, the tunability of periodic artificial gauge potentials is then shown. We discuss the topological properties of the effective model in Sec. IV. In Sec. V we conclude with a discussion.

## II. PROPOSAL

Illuminated by the modulated pumping laser, we consider cold-AEMA gases confined in a one-dimensional driven superlattice, which is illustrated intuitively in Fig. 1(a). The pumping laser interrogates the transition between the ground

states  $|g\rangle$  and the excited states  $|e\rangle$ . Such a superlattice is formed by overlapping two one-dimensional (1D) optical lattices with one at a magic wavelength  $\lambda_m$  giving a lattice depth  $V_m$  and the other at a wavelength  $2\lambda_m$  giving depths  $V_g$  and  $V_e$  for states  $|g\rangle$  and  $|e\rangle$ , respectively. To simplify our discussion, the superlattice and pumping laser are assumed to be driven simultaneously and the sine protocol is chosen, which can be achieved by acousto-optic modulators.

Defining  $\mathcal{P}_g$  and  $\mathcal{P}_e$  as the projection operator to the ground state  $|g\rangle$  and the excited state  $|e\rangle$ , respectively, the driven state-dependent superlattice can be written as

$$V(x, t) = -V_m \cos^2\{k_m[x - X_L(t)]\} \\ - V_g \mathcal{P}_g \cos^2\left(\frac{k_m}{2}[x - X_L(t)]\right) \\ - V_e \mathcal{P}_e \cos^2\left(\frac{k_m}{2}[x - X_L(t)]\right), \quad (1)$$

where the sinusoidal driven function is applied

$$X_L(t) = \frac{\lambda_m}{2} \int_0^t v_1 \sin(\omega_s \tau) d\tau, \quad (2)$$

with  $\omega_s/2\pi$  denoting the driving frequency. The right-hand side of the first line in Eq. (1) indicates that the atomic two levels experience the same lattice potential generated by the magic wavelength  $\lambda_m$ . In contrast, the second and third lines describe different trapping conditions due to the laser with wavelength  $2\lambda_m$ . Assuming identical spatial shaking  $X_L(t)$  for the two lattices, the two driven protocols should be coordinated as shown in Fig. 1(b). Let  $v_1$  be the frequency excursion of the modulation to the magic laser frequency. Such conditions can be achieved by just choosing the frequency excursion  $v_1/2$  for the other one.

Considering another time-dependent modulation to the frequency of the pumping laser,

$$\Delta\nu_p(t) = v_2 \cos(\omega_s t + \varphi) + \frac{1}{\lambda_p} \dot{X}_L(t), \quad (3)$$

which is shown in Fig. 1(c), the  $|g\rangle \leftrightarrow |e\rangle$  transition can be described by the atom-laser coupling matrix (under the rotating-wave approximation)

$$W = \frac{\hbar}{2} \begin{pmatrix} \delta & g e^{ik_p[x - X_p(t)]} \\ g e^{-ik_p[x - X_p(t)]} & -\delta \end{pmatrix},$$

with

$$X_p(t) = \lambda_p \int_0^t d\tau \Delta\nu_p(\tau). \quad (4)$$

Here  $g$  is the Rabi frequency,  $\delta = \omega_0 - \omega_p$  is the detuning,  $\omega_0$  is the frequency difference between  $|g\rangle$  and  $|e\rangle$ , and  $\lambda_p$  and  $k_p$  are the wavelength and wave number of the pumping laser, respectively. It is noteworthy that we have introduced an initial phase difference  $\varphi$  between the two driven functions in Eq. (2), which is the key ingredient for engineering the periodic flux in our following discussion. According to cold-AEMA experiments such as those using  $^{173}\text{Yb}$  [68,70] and  $^{87}\text{Sr}$  [71,73,74], neglecting atomic interaction in some suitable lattices is reasonable. Under individual-particle approximation, then the external and internal motion of the atoms is

governed by the Hamiltonian

$$H = \left( \frac{p^2}{2m} + V(x, t) \right) \otimes \hat{1} + W, \quad (5)$$

where  $m$  and  $p$  are the atomic mass and momentum, respectively, and  $\hat{1}$  is the identity operator associated with the internal atomic degrees of freedom.

### III. EFFECTIVE HAMILTONIAN AND PERIODIC GAUGE FIELDS

It is convenient to work in the frame of reference comoving with the superlattice, into which we can transform the atomic motion by two steps of unitary transformation. First, we define  $U_1 = \exp[\frac{i}{\hbar} X_L(t)p]$  and transform the Hamiltonian in Eq. (5) by  $H \rightarrow H_1 = U_1 H U_1^\dagger - i\hbar U_1 \partial_t U_1^\dagger$ . The shift of position in the potential  $V(x, t)$  is compensated by  $U_1 x U_1^\dagger = x + X_L(t)$ . However, the extra term  $-i\hbar U_1 \partial_t U_1^\dagger$  generates  $-\dot{X}_L(t)p$ , which means a shift of the momentum. To cancel this extra term, we implement the other unitary transformation by  $U_2 = \exp[-\frac{i}{\hbar} m \dot{X}_L(t)x]$ , which results in  $p \rightarrow p + m \dot{X}_L(t)$ . Finally, the Hamiltonian  $H_c = U_2 H_1 U_2^\dagger - i\hbar U_2 \partial_t U_2^\dagger$  in the comoving frame becomes

$$H_c = \left( \frac{p^2}{2m} + V'(x) + m \ddot{X}_L(t)x - \frac{m}{2} \dot{X}_L(t)^2 \right) \otimes \hat{1} + \frac{\hbar}{2} \begin{pmatrix} \delta & g e^{ik_p[x - X_p(t) + X_L(t)]} \\ g e^{-ik_p[x - X_p(t) + X_L(t)]} & -\delta \end{pmatrix}, \quad (6)$$

with the undriven superlattice potential

$$V'(x) = -V_1 \cos^2(k_L x) - V_g \mathcal{P}_g \cos^2\left(\frac{k_L}{2}x\right) - V_e \mathcal{P}_e \cos^2\left(\frac{k_L}{2}x\right). \quad (7)$$

Here the term  $-\frac{m}{2} \dot{X}_L(t)^2$  can be ignored since it is a time-dependent energy shift. In this laboratory frame, we can see now that the vibration of the superlattice gives rise to two physical effects. The first is the inertial force, given by  $F(t) = -m \ddot{X}_L(t)$ , which generates the energy term  $m \ddot{X}_L(t)x$ . The second is the Doppler effect, related to the term  $e^{ik_p X_L(t)}$ .

In the Wannier representation using the tight-binding approximation, the many-body Hamiltonian described by Eq. (6) can be formulated as

$$H_c = \sum_{l, \sigma=g, e} K_\sigma (b_{l, \sigma}^\dagger a_{l, \sigma} + a_{l+1, \sigma}^\dagger b_{l, \sigma} + \text{H.c.}) + \frac{\hbar g}{2} e^{ik_p[X_L(t) - X_p(t)]} \sum_l (e^{i2l\theta} a_{l, e}^\dagger a_{l, g} + e^{i(2l+1)\theta} b_{l, e}^\dagger b_{l, g} + \text{H.c.}) + H_F + H_p, \quad (8)$$

where  $a_{l, \sigma}$  ( $a_{l, \sigma}^\dagger$ ) and  $b_{l, \sigma}$  ( $b_{l, \sigma}^\dagger$ ) denote the fermionic annihilation (creation) operators for atoms occupying the Wannier state at the  $a$  and  $b$  sublattices of the  $l$ th site respectively,  $K_\sigma$  is the corresponding tunneling amplitude, and  $g$  and  $e$  label the internal states  $|g\rangle$  and  $|e\rangle$ , respectively. Here the phase  $\theta = \pi \lambda_m / \lambda_p$  can be changed by adjusting the angle between

the pumping laser and the superlattice [70]. The energies associated with the inertial force acting on atoms at different sites are given by

$$H_F = -F(t) \lambda_m \sum_{l, \sigma=g, e} \left[ l a_{l, \sigma}^\dagger a_{l, \sigma} + \left( l + \frac{1}{2} \right) b_{l, \sigma}^\dagger b_{l, \sigma} \right]. \quad (9)$$

Let  $\mu$  be the chemical potential generated by the magic lattice, the first term on the right-hand in Eq. (7). Then the second and third terms in Eq. (7) will shift the chemical potential of one sublattice (assuming sublattice  $a$ ) to be  $\mu_{a, g}$  and  $\mu_{a, e}$ , respectively. Including the detuning related energy, the corresponding total potentials become  $\mu_{a, g} - \frac{\hbar}{2} \delta$  and  $\mu_{a, e} + \frac{\hbar}{2} \delta$  at  $a$  sites and  $\mu - \frac{\hbar}{2} \delta$  and  $\mu + \frac{\hbar}{2} \delta$  at  $b$  sites. Visualization of those potentials is also sketched in Fig. 1(a). Since we are interested in Floquet photon-assisted resonant processes, we set those potentials equal to integer multiples of  $\hbar \omega_s$ ,

$$H_p = \hbar \omega_s \sum_l [n_a a_{l, e}^\dagger a_{l, e} + m_g b_{l, g}^\dagger b_{l, g} + (n_a + m_e) b_{l, e}^\dagger b_{l, e}], \quad (10)$$

where  $\mu_{a, g} - \frac{\hbar}{2} \delta$  is redefined as the zero point of potential energy and  $n_a \hbar \omega_s = \mu_{a, e} - \mu_{a, g} + \hbar \delta$ ,  $m_g \hbar \omega_s = \mu - \mu_{a, g}$ , and  $m_e \hbar \omega_s = \mu - \mu_{a, e}$ . It is notable that the ratio of  $m_g$  to  $m_e$  is equal to the ratio of the polarizability of the ground state to the excited state at the wavelength  $2\lambda_m$ . By choosing proper driving frequency, lattice laser power, and detuning, this resonant condition can be achieved.

We proceed to discuss the resonant situation. In this case, we need to combine the potentials  $H_p$  with the inertial force induced energies  $H_F$  and the Doppler effect associated terms  $e^{ik_p[X_L(t) - X_p(t)]}$  in Eq. (8). Based on this consideration, we do a combined rotation transformation of  $U_3 = \exp(\frac{i}{\hbar} \int_0^t H_F d\tau)$  and  $U_4 = \exp(\frac{i}{\hbar} H_p t)$ , which leads to the new Hamiltonian

$$H_R = U_4 U_3 H_c U_3^\dagger U_4^\dagger - i\hbar U_4 U_3 \partial_t (U_3^\dagger U_4^\dagger) = \sum_{l, \sigma=g, e} K_\sigma (\eta_{b, a}^\sigma b_{l, \sigma}^\dagger a_{l, \sigma} + \eta_{a, b}^\sigma a_{l+1, \sigma}^\dagger b_{l, \sigma}) + \frac{\hbar g}{2} \sum_l (\chi_a^l a_{l, e}^\dagger a_{l, g} + \chi_b^l e^{i\theta} b_{l, e}^\dagger b_{l, g} + \text{H.c.}), \quad (11)$$

where

$$\eta_{b, a}^\sigma = \exp\left(-\frac{i}{2\hbar} \int_0^t d\tau F(\tau) \lambda_m + i m_\sigma \omega_s t\right),$$

$$\eta_{a, b}^\sigma = \exp\left(-\frac{i}{2\hbar} \int_0^t d\tau F(\tau) \lambda_m - i m_\sigma \omega_s t\right),$$

$$\chi_\alpha^l = \exp\{i2l\theta + ik_p[X_L(t) - X_p(t)] + i n_\alpha \omega_s t\}, \quad (12)$$

with  $\alpha$  denoting  $a$  or  $b$  and  $n_b = n_a + m_e - m_g$ .

In a typical AEMA experiment, for example, on  $^{87}\text{Sr}$  atoms [73, 74], the driving frequency  $\omega_s/2\pi$  can vary from several hundred to several kilohertz and the superlattice depth ranges from near zero to tens of recoil energies (the recoil energy is defined as  $E_r = \hbar^2/2m\lambda_m^2$ ). Therefore, we can adjust the experimental parameters to ensure that the driven frequency is larger than the intersite tunneling amplitudes and the Rabi frequency, and then the high-frequency expansion can be

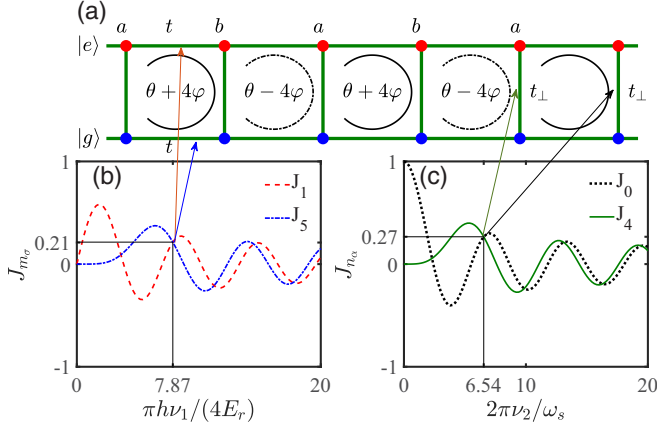


FIG. 2. Illustration of the effective two-leg ladder model with periodic gauge fields. (a) A modulated pumping laser induces transitions between ground states  $|g\rangle$  and excited states  $|e\rangle$ , which can be viewed as two sites in the synthetic dimension. The tunneling between sublattices is inhibited due to the potential offset and can be restored with the assistance of Floquet photons. The Floquet photon-assisted resonance pathways of one loop in each plaquette is accompanied by phases  $\theta$  and  $\varphi$ , thus giving rise to periodic fluxes. (b) Renormalized functions of the hopping amplitudes along the legs are Bessel functions  $J_1$  and  $J_5$ . (c) Renormalized functions along the rungs,  $J_0$  and  $J_4$ .

applied safely. In our proposal, the periodic modulation is a sine signal function, as shown in Eqs. (2) and (3). We make use of the Bessel function expansion  $e^{iz \sin \beta} = \sum_k J_k(z) e^{ik\beta}$  to replace the driven modulation terms in Eq. (12). Keeping only the resonant processes and neglecting other rapidly oscillating terms, the renormalized parameters of Eq. (12) can be approximately expressed as

$$\begin{aligned} \eta_{b,a}^\sigma &\approx J_{-m_\sigma}(\Gamma_1), \\ \eta_{a,b}^\sigma &\approx J_{m_\sigma}(\Gamma_1), \\ \chi_\alpha^l &\approx J_{n_\alpha}(\Gamma_2) e^{2il\theta - in_\alpha\varphi}, \end{aligned} \quad (13)$$

where  $\Gamma_1 = \pi\hbar\nu_1/4E_r$  and  $\Gamma_2 = 2\pi\nu_2/\omega_s$ . Finally, substituting Eq. (13) into Eq. (11), we obtain a time-independent effective Hamiltonian. By employing the internal atomic degrees of freedom as the extra lattice dimension, it can be regarded as a two-leg flux ladder model as depicted in Fig. 2(a).

From the last of Eqs. (13) we can see that the phases  $n_\alpha\varphi$ , and thus the relevant gauge fields, emerge from the internal state resonant transition with the assistance of Floquet photons. As for this artificial gauge field, the physical gauge-invariant quantity is the phase accumulated on an elementary loop per plaquette. Taking into account the phase  $\theta$ , the total magnetic flux through each plaquette is  $\theta \pm (n_a - n_b)\varphi$ . For an atomic species such as  $^{87}\text{Sr}$ , the polarizability  $\alpha_e$  of the  $|e\rangle$  states at the wavelength  $2\lambda_m \approx 1626.86$  nm is 41.36 a.u. [75]. Choosing a proper laser power of wavelength  $2\lambda_m$ , the relevant chemical potential shift of the  $|e\rangle$  state can be matched to the driving frequency as  $\mu - \mu_{a,e} \approx \alpha_e E^2 \approx \hbar\omega_s = h \times 1$  kHz, namely,  $m_e = 1$ . Note that the polarizability  $\alpha_g$  of  $|g\rangle$  states is 206.37 a.u., which is approximately five times that of the  $|e\rangle$  state, and then  $\mu - \mu_{a,g} \approx \alpha_g E^2 \approx h \times 5$  kHz and  $m_g = 5$ . Setting the detuning  $\delta$  to zero, which implies  $n_b = 0$

and  $n_a = 4$ , the accumulated phase is  $\theta \pm 4\varphi$  in this case. Now it is clear that our scheme can simulate the periodic  $U(1)$  gauge fields with two plaquettes as one period. Recall that  $\theta$  is induced by an incommensurate ratio between wavelengths of the lattice and the pumping lasers; it can be tuned by adjusting the angle between those lasers. Moreover,  $\varphi$  is the initial phase of the sinusoidal driving function and is fully controllable [73]. Thus our scheme offers a feasible method to tune the periodic gauge potentials.

Finally, we discuss the modulation of hopping amplitudes in the effective model. The Bessel functions from Eq. (13) renormalize the nearest-neighbor hopping amplitudes along legs as  $K_\sigma J_{m_\sigma} (0.25\pi\hbar\nu_1/E_r)$  and along rungs as  $\frac{1}{2}\hbar g J_{n_\alpha} (2\pi\nu_2/\omega_s)$ , respectively. Independent of the phases  $\theta$  and  $\varphi$ , such simple parameter-dependent function forms result in their individual controllability via varying the driving amplitudes  $\nu_1$  and  $\nu_2$ . While the demonstrated controllability offers exciting possibilities, it is essential to first consider the widely studied cases with equal hopping amplitudes along legs and along rungs. Figure 2(b) shows the Bessel functions  $J_{m_\sigma}$  for  $m_g = 5$  and  $m_e = 1$ . The crossing points  $J_5(\Gamma_1) = J_1(\Gamma_1)$  indicate the equal tunneling amplitudes along legs if considering  $K_g \approx K_e$ . Similarly, Fig. 2(c) illustrates the tuned hopping amplitudes across rungs, with equal points clearly visible.

#### IV. TOPOLOGICAL PHASE

Now we investigate the topological phase of the ladder model caused by the gauge fields. For clarity, we rewrite the effective Hamiltonian for the case of  $m_g = 5$ ,  $m_e = 1$ ,  $n_a = 4$ , and  $n_b = 0$ ,

$$\begin{aligned} H_{\text{eff}} = &t \sum_l (e^{i(\theta+\phi)} b_{l,g}^\dagger a_{l,g} + e^{i(\theta-\phi)} a_{l+1,g}^\dagger b_{l,g} \\ &+ b_{l,e}^\dagger a_{l,e} + a_{l+1,e}^\dagger b_{l,e}) \\ &+ t_\perp \sum_l (a_{l,e}^\dagger a_{l,g} + b_{l,e}^\dagger b_{l,g}) + \text{H.c.}, \end{aligned} \quad (14)$$

where  $t = 0.21K_\sigma$ ,  $t_\perp = 0.14\hbar g$ ,  $\phi = 4\varphi$ , and the proper gauge transformation is performed. When  $\phi = 0$ , namely, the uniform flux scenario, previous research has demonstrated that no topological states are present in this 1D system [76]. When  $\theta + \phi = 0$  and  $\theta - \phi = \pi$ , recent work by Jiang *et al.* shows that nontrivial topological states manifest and the topological invariant can be entirely determined by the projective symmetry algebra [32]. For  $\phi/2\pi$  being the rational number, Sun [25] studied the particular case of periodic fluxes with period 3,  $\Omega_1 = \theta + 2\pi/3$ ,  $\Omega_2 = \theta + 4\pi/3$ , and  $\Omega_3 = \theta + 2\pi$ , where the 1D topological invariant was elucidated with the help of the Chern numbers of the corresponding extended 2D system.

To explore the effects of general periodic gauge fields in Eq. (14), we notice that this model exhibits combined symmetry of inversion  $P$  and time reversal  $T$ :

$$PTH_{\text{eff}}(PT)^{-1} = H_{\text{eff}}. \quad (15)$$

In momentum space, the Hamiltonian and  $PT$  operator are represented by

$$H_{\text{eff}} = t \begin{pmatrix} 1 + \cos(k) & 0 \\ 0 & \cos(\theta + \phi) + \cos(k - \theta + \phi) \end{pmatrix} \otimes \sigma_1 \\ + t \begin{pmatrix} \sin(k) & 0 \\ 0 & \sin(\theta + \phi) + \sin(k - \theta + \phi) \end{pmatrix} \otimes \sigma_2 \\ + t_{\perp} \tau_1 \otimes \sigma_0, \\ PT = \tau_0 \otimes \sigma_1 \mathcal{K}, \quad (16)$$

respectively, where  $\tau_i$  and  $\sigma_i$  denote Pauli matrices and  $\mathcal{K}$  denotes the complex conjugation. Since  $(PT)^2 = 1$ , the  $PT$  operator can be transformed into  $\mathcal{K}$  by a unitary transformation, and the corresponding Hamiltonian  $H_{\text{eff}}(k)$  will be required to be real in this basis. When the number of occupied bands is 1 or 3, the ground state is classified by the first Stiefel-Whitney class and characterized by a  $\mathbb{Z}_2$ -valued topological invariant [77,78]. The topological invariant  $\nu$  can be formulated with the help of the Wilson loop. Introducing the non-Abelian gauge connection  $[A(k)]_{ab} = \langle u_a(k) | \partial_k | u_b(k) \rangle$ , where  $|u_a(k)\rangle$  and  $|u_b(k)\rangle$  are the wave functions of occupied bands, the Wilson loop is constructed as

$$W = P \exp \left( \int_{-\pi}^{\pi} A(k) dk \right), \quad (17)$$

where  $P$  indicates path ordering. Here  $\nu$  is defined by the determinate of  $W$ ,

$$(-1)^\nu = \det W = \prod_j e^{i\alpha_j}, \\ \nu = \frac{1}{\pi} \sum_j \alpha_j \text{mod} 2, \quad (18)$$

where  $e^{i\alpha_j}$  are eigenvalues of  $W$ . Due to the  $PT$  symmetry,  $\nu$  can only take value 0 or 1 [78].

Taking  $^{87}\text{Sr}$  atoms as an example,  $\theta$  can be approximated as  $7\pi/6$  if the pumping laser is parallel to the lattice laser [71,74]. We set  $t_{\perp}/t = 4$  and restrict  $\phi$  within the interval  $[-\pi, \pi]$  because of its periodicity. Applying  $\mathbb{Z}_2$ -invariant formulas in Eqs. (17) and (18) to the lowest filled band of the Hamiltonian in Eq. (16), we find that  $\nu = 1$  for  $-\pi < \phi < 0$  and is trivial otherwise, as shown in Fig. 3(a). The topological number can be explained as follows [78]. Considering the lowest band of the energy spectrum [see Fig. 3(b)], if we impose real conditions on the bulk wave function over the Brillouin zone, the wave function can be made smooth over  $-\pi < k < \pi$  and glued on the boundaries  $k = \pm\pi$  but with an orientation-reversing transition function. The transition function equal to 1 indicates that the state is orientable and  $\nu = 0$ , while  $-1$  indicates that the state is nonorientable and  $\nu = 1$ , as intuitively depicted in Fig. 3(d). Figure 3(c) shows the probability of a pair of edge states located inside the energy gap separating the second band from the lowest one, calculated for 40 unit cells with open boundary conditions when  $\phi = -\pi/4$ . When  $\phi = 0$ , the system simplifies to the case of uniform fluxes, and the number of sites per unit cell reduces from 4 to 2. This reduction indicates that the energy gap should close when  $\phi = 0$ , which corresponds to a topological phase transition.

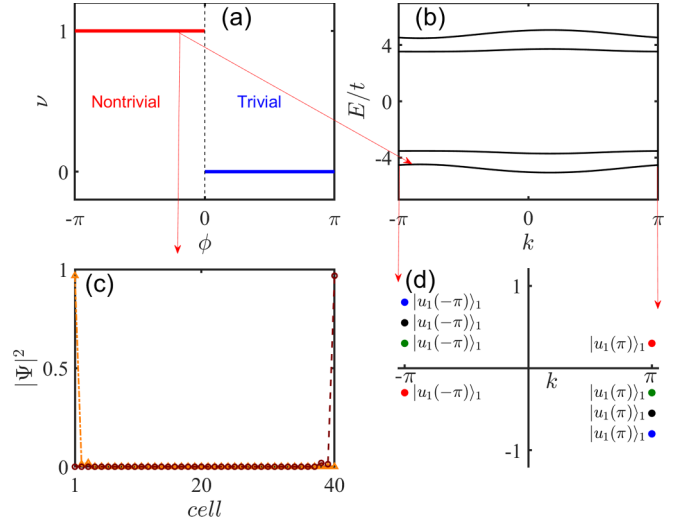


FIG. 3. (a) Topological phase diagram and  $\mathbb{Z}_2$ -invariant  $\nu$  versus  $\phi$ , where  $\theta = 7\pi/6$  and  $t_{\perp}/t = 4$ . (b) Dispersion relation with the same parameters as in (a) but  $\phi = -\pi/4$ , where the topological number of the lowest band  $\nu = 1$ . (c) Pair of edge states corresponding to  $\nu = 1$  in (a) with  $\phi = -\pi/4$ , calculated for 40 unit cells in open boundary conditions. (d) Intuitive illustration of the nonorientable state in the lowest band on the Brillouin zone boundaries  $k = \pm\pi$ .

Additionally, we note that a similar discussion of topological properties can be conducted for three occupied bands, yielding the same results as those for one occupied band. Similar to other well-known topological phases, one observable consequence of this  $PT$  symmetry-protected topological phase is the edge states. However, different from a single band with a nontrivial Zak phase, the topological number  $\nu$  here can be defined for multiple bands. For instance, when there are three occupied bands in our model and  $\nu = 1$ , there will be a pair of edge modes in the third gap.

## V. CONCLUSION

We have presented a feasible and efficient proposal for engineering a two-leg ladder model with periodic gauge fields based on driven cold-AEMA optical lattice systems. The periodic gauge field is widely controllable by independently changing the parameters of the driven protocol. Our proposal can simulate a real topological phase described by the first Stiefel-Whitney class and demonstrate a topological phase transition induced by gauge fields. Furthermore, from an experimental technical perspective, it has a long history of utilizing AEMAs in the construction of optical lattice clocks [79]. The technologies developed for those purpose can be naturally transferred to the study of our proposed gauge field simulation. Therefore, we hope this work could enrich the gauge-field-related topological research both in theory and in future experiments.

One seemingly inevitable obstruction toward realizing the present scheme is the ultimate thermalization of the driven system. However, there is a Floquet prethermal regime where the effect can be employed to describe the system's physics. Generally, the heating rate is exponentially suppressed to

increase the shaking frequency and this prethermal timescale can be engineered up to  $10^4$  driving periods [41,80–82]. The preparation of the sample and the measurement can usually be completed within  $10^2$  cycles [83]. Meanwhile, AEMA's internal states used here have a long lifetime. Thus our scheme is robust and the experimental studies can be completed before the thermalization happens.

Recently, the time-dependent synthetic gauge potentials was theoretically confirmed as the critical ingredient for realizing tailored dynamical evolution of quasiparticles, quasiholes [67,84,85], wave packets [86,87], and adiabatic

state preparation [88]. Another application of our proposal is expected for those dynamical process studies.

### ACKNOWLEDGMENTS

This work was supported by the National Science Foundation of China under Grant No. 12274045. T.W. acknowledges funding from the National Science Foundation of China under Grants No. 12347101 and from the Program of State Key Laboratory of Quantum Optics and Quantum Optics Devices under Grant No. KF202211.

- 
- [1] K. v. Klitzing, G. Dorda, and M. Pepper, *Phys. Rev. Lett.* **45**, 494 (1980).
- [2] R. B. Laughlin, *Phys. Rev. B* **23**, 5632 (1981).
- [3] D. J. Thouless, M. Kohmoto, M. P. Nightingale, and M. D. Nijs, *Phys. Rev. Lett.* **49**, 405 (1982).
- [4] D. C. Tsui, H. L. Stormer, and A. C. Gossard, *Phys. Rev. Lett.* **48**, 1559 (1982).
- [5] R. B. Laughlin, *Phys. Rev. Lett.* **50**, 1395 (1983).
- [6] M. Z. Hasan and C. L. Kane, *Rev. Mod. Phys.* **82**, 3045 (2010).
- [7] X.-L. Qi and S.-C. Zhang, *Rev. Mod. Phys.* **83**, 1057 (2011).
- [8] C.-K. Chiu, J. C. Y. Teo, A. P. Schnyder, and S. Ryu, *Rev. Mod. Phys.* **88**, 035005 (2016).
- [9] A. Bansil, H. Lin, and T. Das, *Rev. Mod. Phys.* **88**, 021004 (2016).
- [10] N. P. Armitage, E. J. Mele, and A. Vishwanath, *Rev. Mod. Phys.* **90**, 015001 (2018).
- [11] F. D. M. Haldane, *Phys. Rev. Lett.* **61**, 2015 (1988).
- [12] K. Ohgushi, S. Murakami, and N. Nagaosa, *Phys. Rev. B* **62**, R6065 (2000).
- [13] K. Sun, Z. Gu, H. Katsura, and S. Das Sarma, *Phys. Rev. Lett.* **106**, 236803 (2011).
- [14] T. Neupert, L. Santos, C. Chamon, and C. Mudry, *Phys. Rev. Lett.* **106**, 236804 (2011).
- [15] W.-C. Chen, R. Liu, Y.-F. Wang, and C.-D. Gong, *Phys. Rev. B* **86**, 085311 (2012).
- [16] R.-C. Ge and M. Kolodrubetz, *Phys. Rev. B* **104**, 035427 (2021).
- [17] D.-H. Guan, L. Qi, X. Zhang, Y. Liu, and A.-L. He, *Phys. Rev. B* **108**, 085121 (2023).
- [18] Z.-Y. Lan, A.-L. He, and Y.-F. Wang, *Phys. Rev. B* **107**, 235116 (2023).
- [19] G. Xu, B. Lian, and S.-C. Zhang, *Phys. Rev. Lett.* **115**, 186802 (2015).
- [20] S.-J. Zhang, C.-W. Zhang, S.-F. Zhang, W.-X. Ji, P. Li, P.-J. Wang, S.-S. Li, and S.-S. Yan, *Phys. Rev. B* **96**, 205433 (2017).
- [21] A.-L. He, W.-W. Luo, Y. Zhou, Y.-F. Wang, and H. Yao, *Phys. Rev. B* **105**, 235139 (2022).
- [22] A.-L. He, X. Zhang, and Y. Liu, *Phys. Rev. B* **106**, 125147 (2022).
- [23] R. Liu, W.-C. Chen, Y.-F. Wang, and C.-D. Gong, *J. Phys.: Condens. Matter* **24**, 305602 (2012).
- [24] Y.-F. Wang and C.-D. Gong, *Phys. Rev. Lett.* **98**, 096802 (2007).
- [25] G. Sun, *Phys. Rev. A* **93**, 023608 (2016).
- [26] H. Cai, J. Liu, J. Wu, Y. He, S.-Y. Zhu, J.-X. Zhang, and D.-W. Wang, *Phys. Rev. Lett.* **122**, 023601 (2019).
- [27] Y. X. Zhao, Y.-X. Huang, and S. A. Yang, *Phys. Rev. B* **102**, 161117(R) (2020).
- [28] L. B. Shao, Q. Liu, R. Xiao, S. A. Yang, and Y. X. Zhao, *Phys. Rev. Lett.* **127**, 076401 (2021).
- [29] Z. Y. Chen, S. A. Yang, and Y. X. Zhao, *Nat. Commun.* **13**, 2215 (2022).
- [30] Z. Y. Chen, Z. Zhang, S. A. Yang, and Y. X. Zhao, *Nat. Commun.* **14**, 743 (2023).
- [31] C. Zhang, Z. Y. Chen, Z. Zhang, and Y. X. Zhao, *Phys. Rev. Lett.* **130**, 256601 (2023).
- [32] G. Jiang, Z. Y. Chen, S. J. Yue, W. B. Rui, X.-M. Zhu, S. A. Yang, and Y. X. Zhao, *Phys. Rev. B* **109**, 115155 (2024).
- [33] Y. X. Zhao, C. Chen, X.-L. Sheng, and S. A. Yang, *Phys. Rev. Lett.* **126**, 196402 (2021).
- [34] H. Xue, Z. Wang, Y.-X. Huang, Z. Cheng, L. Yu, Y. X. Foo, Y. X. Zhao, S. A. Yang, and B. Zhang, *Phys. Rev. Lett.* **128**, 116802 (2022).
- [35] H. Xue, Z. Y. Chen, Z. Cheng, J. X. Dai, Y. Long, Y. X. Zhao, and B. Zhang, *Nat. Commun.* **14**, 4563 (2023).
- [36] J. Dalibard, F. Gerbier, G. Juzeliūnas, and P. Öhberg, *Rev. Mod. Phys.* **83**, 1523 (2011).
- [37] N. Goldman, G. Juzeliūnas, P. Öhberg, and I. B. Spielman, *Rep. Prog. Phys.* **77**, 126401 (2014).
- [38] S. L. Zhang and Q. Zhou, *J. Phys. B* **50**, 222001 (2017).
- [39] M. Aidelsburger, *J. Phys. B* **51**, 193001 (2018).
- [40] V. Galitski, G. Juzeliūnas, and I. B. Spielman, *Phys. Today* **72** (1), 38 (2019).
- [41] C. Weitenberg and J. Simonet, *Nat. Phys.* **17**, 1342 (2021).
- [42] M. R. Matthews, B. P. Anderson, P. C. Haljan, D. S. Hall, C. E. Wieman, and E. A. Cornell, *Phys. Rev. Lett.* **83**, 2498 (1999).
- [43] K. W. Madison, F. Chevy, W. Wohlleben, and J. Dalibard, *Phys. Rev. Lett.* **84**, 806 (2000).
- [44] J. R. Abo-Shaeer, C. Raman, J. M. Vogels, and W. Ketterle, *Science* **292**, 476 (2001).
- [45] P. Engels, I. Coddington, P. C. Haljan, V. Schweikhard, and E. A. Cornell, *Phys. Rev. Lett.* **90**, 170405 (2003).
- [46] V. Schweikhard, I. Coddington, P. Engels, V. P. Mogendorff, and E. A. Cornell, *Phys. Rev. Lett.* **92**, 040404 (2004).
- [47] J. Ruostekoski, G. V. Dunne, and J. Javanainen, *Phys. Rev. Lett.* **88**, 180401 (2002).
- [48] D. Jaksch and P. Zoller, *New J. Phys.* **5**, 56 (2003).
- [49] W. Yi, A. J. Daley, G. Pupillo, and P. Zoller, *New J. Phys.* **10**, 073015 (2008).
- [50] F. Gerbier and J. Dalibard, *New J. Phys.* **12**, 033007 (2010).

- [51] A. Celi, P. Massignan, J. Ruseckas, N. Goldman, I. B. Spielman, G. Juzeliūnas, and M. Lewenstein, *Phys. Rev. Lett.* **112**, 043001 (2014).
- [52] M. Aidelsburger, M. Atala, S. Nascimbène, S. Trotzky, Y.-A. Chen, and I. Bloch, *Phys. Rev. Lett.* **107**, 255301 (2011).
- [53] A. Eckardt, C. Weiss, and M. Holthaus, *Phys. Rev. Lett.* **95**, 260404 (2005).
- [54] H. Lignier, C. Sias, D. Ciampini, Y. Singh, A. Zenesini, O. Morsch, and E. Arimondo, *Phys. Rev. Lett.* **99**, 220403 (2007).
- [55] A. Zenesini, H. Lignier, D. Ciampini, O. Morsch, and E. Arimondo, *Phys. Rev. Lett.* **102**, 100403 (2009).
- [56] J. Struck, C. Olschlager, R. L. Targat, P. Soltan-Panahi, A. Eckardt, M. Lewenstein, P. Windpassinger, and K. Sengstock, *Science* **333**, 996 (2011).
- [57] P. Hauke, O. Tieleman, A. Celi, C. Olschlager, J. Simonet, J. Struck, M. Weinberg, P. Windpassinger, K. Sengstock, M. Lewenstein, and A. Eckardt, *Phys. Rev. Lett.* **109**, 145301 (2012).
- [58] K. Jiménez-García, L. J. LeBlanc, R. A. Williams, M. C. Beeler, A. R. Perry, and I. B. Spielman, *Phys. Rev. Lett.* **108**, 225303 (2012).
- [59] N. Goldman and J. Dalibard, *Phys. Rev. X* **4**, 031027 (2014).
- [60] M. Bukov, M. Kolodrubetz, and A. Polkovnikov, *Phys. Rev. Lett.* **116**, 125301 (2016).
- [61] K. Plekhanov, G. Roux, and K. Le Hur, *Phys. Rev. B* **95**, 045102 (2017).
- [62] J. Struck, C. Olschlager, M. Weinberg, P. Hauke, J. Simonet, A. Eckardt, M. Lewenstein, K. Sengstock, and P. Windpassinger, *Phys. Rev. Lett.* **108**, 225304 (2012).
- [63] A. Eckardt, *Rev. Mod. Phys.* **89**, 011004 (2017).
- [64] J. Struck, M. Weinberg, C. Olschlager, P. Windpassinger, J. Simonet, K. Sengstock, R. Hoppner, P. Hauke, A. Eckardt, M. Lewenstein, and L. Mathey, *Nat. Phys.* **9**, 738 (2013).
- [65] G. Jotzu, M. Messer, R. Desbuquois, M. Lebrat, T. Uehlinger, D. Greif, and T. Esslinger, *Nature (London)* **515**, 237 (2014).
- [66] N. Fläschner, B. S. Rem, M. Tarnowski, D. Vogel, D. S. Luhmann, K. Sengstock, and C. Weitenberg, *Science* **352**, 1091 (2016).
- [67] B. T. Wang, F. N. Únal, and A. Eckardt, *Phys. Rev. Lett.* **120**, 243602 (2018).
- [68] M. Mancini, G. Pagano, G. Cappellini, L. Livi, M. Rider, J. Catani, C. Sias, P. Zoller, M. Inguscio, M. Dalmonte, and L. Fallani, *Science* **349**, 1510 (2015).
- [69] M. L. Wall, A. P. Koller, S. Li, X. Zhang, N. R. Cooper, J. Ye, and A. M. Rey, *Phys. Rev. Lett.* **116**, 035301 (2016).
- [70] L. F. Livi, G. Cappellini, M. Diem, L. Franchi, C. Clivati, M. Frittelli, F. Levi, D. Calonico, J. Catani, M. Inguscio, and L. Fallani, *Phys. Rev. Lett.* **117**, 220401 (2016).
- [71] S. Kolkowitz, S. L. Bromley, T. Bothwell, M. L. Wall, G. E. Marti, A. P. Koller, X. Zhang, A. M. Rey, and J. Ye, *Nature (London)* **542**, 66 (2017).
- [72] S. L. Bromley, S. Kolkowitz, T. Bothwell, D. Kedar, A. Safavi-Naini, M. L. Wall, C. Salomon, A. M. Rey, and J. Ye, *Nat. Phys.* **14**, 399 (2018).
- [73] X.-T. Lu, T. Wang, T. Li, C.-H. Zhou, M.-J. Yin, Y.-B. Wang, X.-F. Zhang, and H. Chang, *Phys. Rev. Lett.* **127**, 033601 (2021).
- [74] M.-J. Yin, X.-T. Lu, T. Li, J.-J. Xia, T. Wang, X.-F. Zhang, and H. Chang, *Phys. Rev. Lett.* **128**, 073603 (2022).
- [75] R.-S. Han, W. Wang, and T. Wang, *Chin. Phys. B* **33**, 043201 (2024).
- [76] D. Hügél and B. Paredes, *Phys. Rev. A* **89**, 023619 (2014).
- [77] C. Fang, Y. Chen, H.-Y. Kee, and L. Fu, *Phys. Rev. B* **92**, 081201(R) (2015).
- [78] J. Ahn, D. Kim, Y. Kim, and B.-J. Yang, *Phys. Rev. Lett.* **121**, 106403 (2018).
- [79] A. D. Ludlow, M. M. Boyd, J. Ye, E. Peik, and P. O. Schmidt, *Rev. Mod. Phys.* **87**, 637 (2015).
- [80] T. Mori, T. N. Ikeda, E. Kaminishi, and M. Ueda, *J. Phys. B* **51**, 112001 (2018).
- [81] M. Messer, K. Sandholzer, F. Görg, J. Minguzzi, R. Desbuquois, and T. Esslinger, *Phys. Rev. Lett.* **121**, 233603 (2018).
- [82] A. Rubio-Abadal, M. Ippoliti, S. Hollerith, D. Wei, J. Rui, S. L. Sondhi, V. Khemani, C. Gross, and I. Bloch, *Phys. Rev. X* **10**, 021044 (2020).
- [83] T. Wang, S. Hu, S. Eggert, M. Fleischhauer, A. Pelster, and X.-F. Zhang, *Phys. Rev. Res.* **2**, 013275 (2020).
- [84] M. Račiūnas, F. N. Únal, E. Anisimovas, and A. Eckardt, *Phys. Rev. A* **98**, 063621 (2018).
- [85] B. Wang, X.-Y. Dong, and A. Eckardt, *SciPost Phys.* **12**, 095 (2022).
- [86] F. Yılmaz and M. Ö. Oktel, *Phys. Rev. A* **97**, 023612 (2018).
- [87] K. Lelas, O. Čelan, D. Prelogović, H. Buljan, and D. Jukić, *Phys. Rev. A* **103**, 013309 (2021).
- [88] B. Wang, X.-Y. Dong, F. N. Únal, and A. Eckardt, *New J. Phys.* **23**, 063017 (2021).